# Nonequilibrium pattern formation in the crystallization of polymer blend films

Vincent Ferreiro,[1,*] Jack F. Douglas,[1,*] James A. Warren,[2] and Alamgir Karim[1]
[1]*Polymers Division, National Institute of Standards and Technology, Gaithersburg, Maryland 20899*
[2]*Metallurgy Division, National Institute of Standards and Technology, Gaithersburg, Maryland 20899*
(Received 15 March 2001; revised manuscript received 10 December 2001; published 2 April 2002)

We show that the morphology of polyethylene oxide crystallization in thin films can be *tuned* to obtain circular spherulites, seaweed and symmetric dendrites, and fractal aggregation forms through the addition of clay particles and the amorphous polymer, polymethyl methacrylate. The thin-film polymer crystallization patterns are compared to a two-dimensional phase field model of dendritic growth in Ni/Cu alloys with a variable surface tension anisotropy $\varepsilon$. Some aspects of polymer crystallization patterns can be understood from the phase field calculations, but a more general model is required to describe the full range of observed patterns.

DOI: 10.1103/PhysRevE.65.042802 PACS number(s): 83.80.Tc, 47.54.+r, 81.10.Aj, 61.43.Hv

A competition between orderly and disorderly growth occurs in a wide range of pattern formation processes (growth of cell colonies, electrochemical deposition, etc., [1]). To better understand nonequilibrium pattern formation, and polymer and metal crystallization, in particular, it is important to have experimental and computational model systems that can be ''tuned'' through the recognized class of pattern types [1,2] and to determine the interactions and processes that govern this type of pattern formation.

Pattern formation in nonequilibrium crystallization is predicted to depend on the degree of undercooling and a parameter governing the intensity of the expression of crystalline symmetry in the pattern formation, the surface tension anisotropy $\varepsilon$ [2]. However, there have been no experimental investigations of crystallization in which $\varepsilon$ is varied to check predictions of recent theories of nonequilibrium crystal growth. Most recent studies of nonequilibrium crystallization have been restricted to simple organic fluids (e.g., succinonitrile) where $\varepsilon$ does not vary appreciably [3]. Moreover, these studies are ordinarily limited to relatively low undercooling to allow measurements of the kinetics of crystal growth by optical microscopy. Polymeric materials have the advantage that the crystallization rate is usually much smaller than metals and small molecule liquids and it is often possible to study crystallization at high undercooling. We investigate thin blend films of a crystalline polymer [polyethlene oxide (PEO)] and an amorphous polymer [polymethyl methacrylate (PMMA)]. The films are sufficiently thin (thickness $\leqslant$200 nm) to be treated as nearly two dimensional [4].

PMMA and PEO materials were purchased from Aldrich [5] and their polydispersity indices $k$ ($k=M_w/M_n$) were determined at NIST by gel permeation chromatography to equal $k(\mathrm{PMMA})=1.8$ ($M_w=7.3\times10^3$ g mol$^{-1}$ [6]) and $k(\mathrm{PEO})$ ($M_w=1.5\times10^5$ g mol$^{-1}$ [6]) $\approx$4. The equilibrium melting temperature $T_m$ of pure PEO was determined to equal $T_m=338$ K by differential-scanning calorimetry on thick (20 $\mu$m) evaporated PEO/chloroform films and the glass transition temperatures $T_g$ of the PEO and PMMA films equal 213 and 377 K, respectively. ''Cloisite'' (montmorillonite) clay particles were obtained from Southern Clay Products [5]. We placed 1 g of clay and 50 ml of distilled water in a 100-ml beaker at 353 K, and 1 g of distearyldimethyl ammonium chloride was then added to the solution. The blend components (PEO/PMMA/clay) were dissolved in chloroform at a total concentration of 1% by mass ratio, unless otherwise stated. The clay concentration of the spin-casting solution was fixed at 5% of the mass of the blend. Thin blend films with the clay additive were spin coated onto Si substrates (Semiconductor Processing Co., orientation (100), Type *P* [5]) at a spin speed of 2000 rpm, resulting in films of uniform thickness (200 nm) unless otherwise stated. After spin casting, the blend films were melted at 373 K for 10 min and then cooled to the crystallization temperature $T_c$. Reflective optical micrographs (OM) were obtained using a Nikon optical microscope (OM) with a digital Kodak MegaPlus charge coupled device camera attachment [5]. Miscibility characteristics are discussed elsewhere [7,8].

In Fig. 1, we show that the crystallization morphology of PEO/PMMA blend films can be tuned by varying the polymer composition at a fixed temperature ($T_c=305$ K). The PEO melting temperature ($T_m$) depends on the polymer composition and $T_m$ values are indicated in the caption, along with the dimensionless undercooling, $\delta T=(T_m-T_c)/T_m$. Clay particles nucleate the crystallization and are apparent as dark spots at the center of the patterns.

Over a large range of PEO mass fraction (50–100 % PEO by mass), we find [Fig. 1(a)] circularly symmetric spherulites. This is the ''normal'' polymer crystallization morphology encountered under processing conditions [9]. The needlelike branches of the spherulite become increasingly coarse with increasing PMMA concentration and the inset to Fig. 1(a) shows a magnified view of this spherulite microstructure for a 70/30 blend (ratio indicates PEO/PMMA mass ratio). Recent studies of nonequilibrium crystallization in electrodeposition indicate that noisy convection at high rates of crystal growth *suppresses* tip splitting, leading to symmetric spherulitelike growth [10]. We anticipate that fluctuations in the stress field about a rapidly growing crystallization front can lead to similar effects in highly viscous polymer fluids, but we leave this question to future study.

In a composition range between 50/50 and 40/60, we observe a transition between the spherulite and *seaweed den-*

*Author to whom correspondence should be addressed.

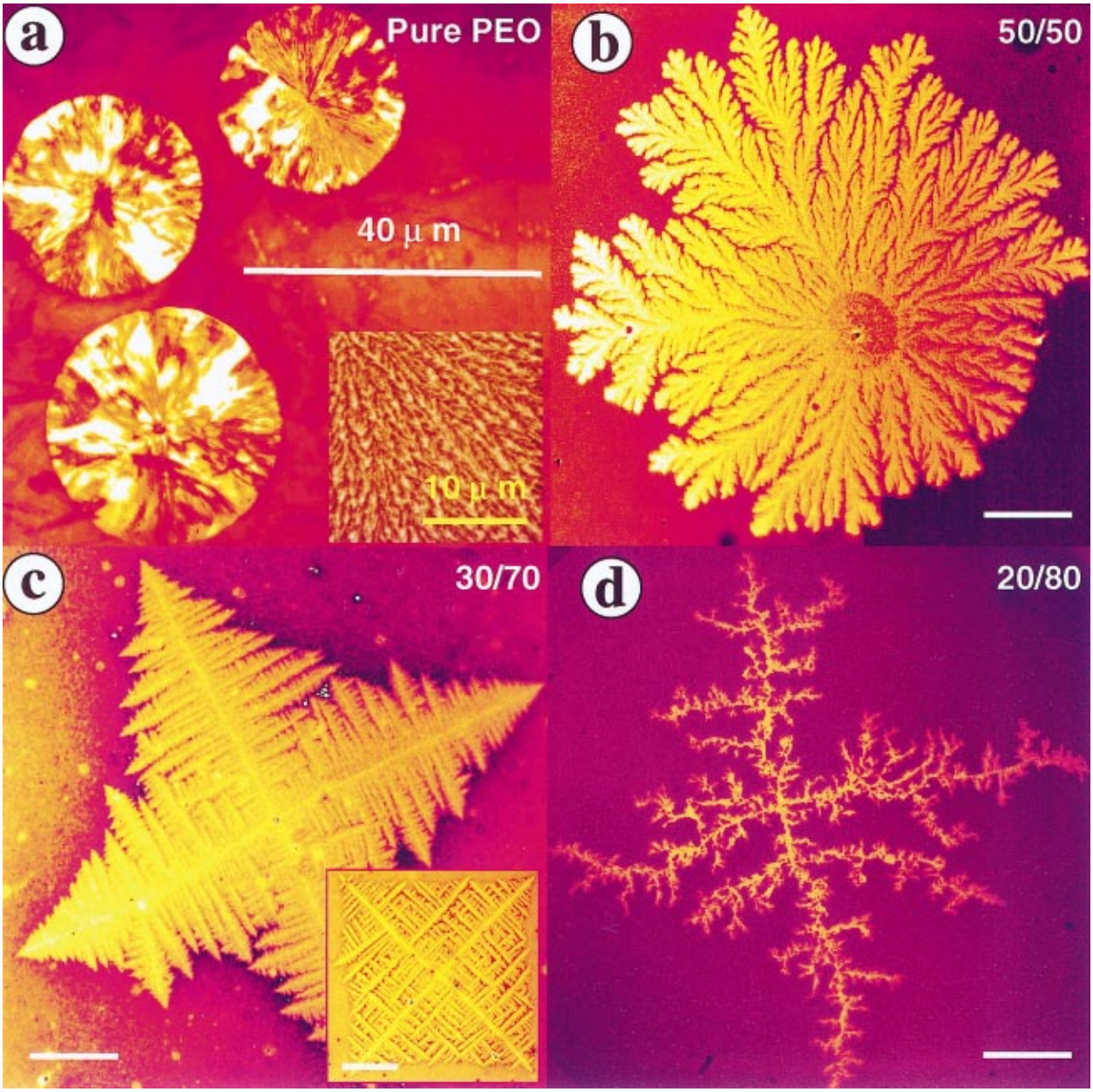


FIG. 1. (Color) Polymer crystallization morphologies as a function of polymer composition. OM images rendered in false color and $h \approx 200$ nm, unless otherwise noted. (a) Spherulitic crystallization of a pure PEO film ($T_m = 340$ K, $\delta T = 0.09$). The needlelike substructure becomes coarser in the spherulite regime with increasing PMMA concentration. Inset shows this substructure for a 70/30 blend. (b) Seaweed dendritic growth in a (50/50) PEO-PMMA film ($T_m = 332$ K, $\delta T = 0.07$). (c) Symmetric dendritic growth in a (30/70) PEO-PMMA film. Inset shows crystallization morphology for 50-nm film. (d) Fractal dendritic growth pattern in a (20/80) PEO-PMMA. $T_m$ was determined by differential scanning calorimetry on 20-$\mu$m-thick evaporated films. The relative clay polymer mass has been fixed at 5%.

*drite* morphologies [Fig. 1(b)] [11]. Seaweed growth is characterized by broad growing tips that split intermittently. After splitting, one of the newly formed branches normally grows to predominate over the other. Repeating this process leads to a cascade of branching events and to a crystallization pattern resembling seaweed and other natural growth forms [1]. The dynamics of this type of growth has recently been investigated by Utter, Ragnarsson, and Bodenschatz [12].

Increasing the PMMA concentration further to the range 40/60–30/70 yields another morphological transition. In this concentration range, we observe well-formed *symmetric dendrites* where the fourfold symmetry of equilibrium PEO crystallization asserts itself at a macroscopic scale [Fig. 1(c)] [13]. Note the near registry of the sidebranches on each side of the growing dendrite arm and the uniformity of the ''starlike'' envelope curve describing the positions of the sidebranch tips of the dendrite [14]. The shape of the dendrite envelope remains nearly *invariant* after an early transient regime [8]. This highly regular structure is reminiscent of symmetric dendritic crystallization driven by periodic external perturbations [15].

A separate paper focuses on the growth dynamics of the

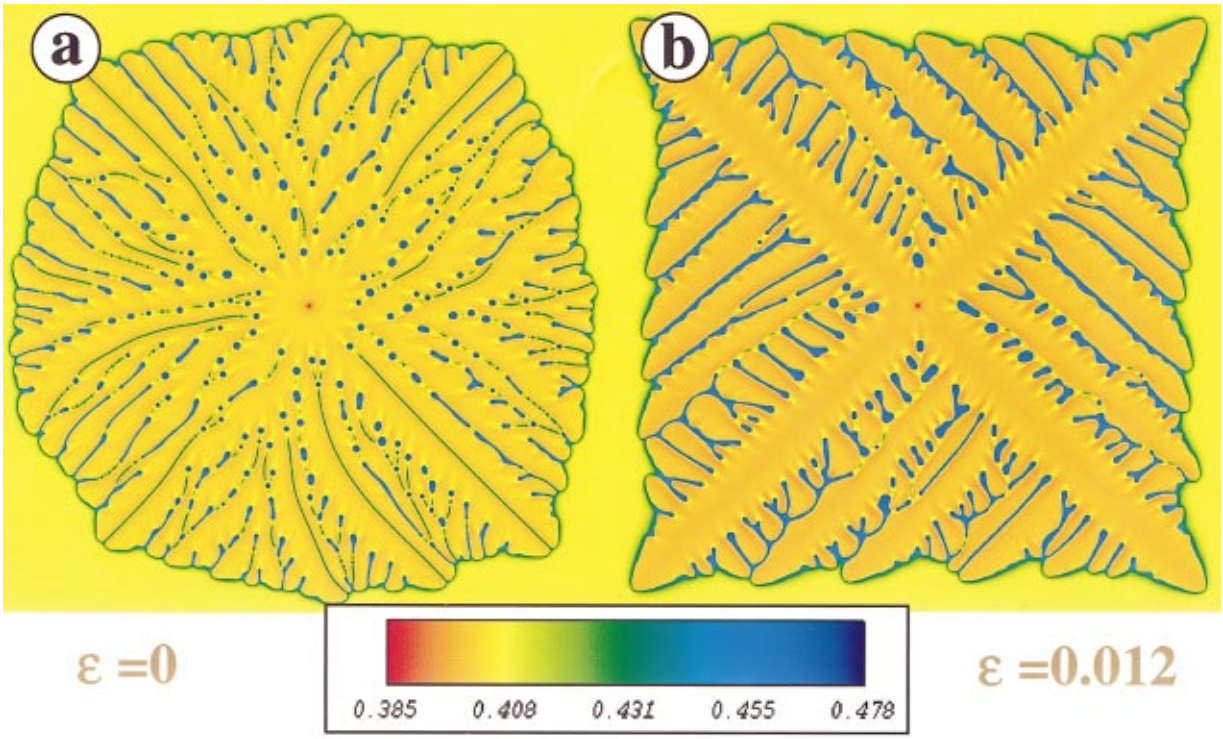


FIG. 2. (Color) Influence of surface tension anisotropy $\varepsilon$ on phase field simulations of dendritic crystallization of a model alloy mixture. (a) Seaweed dendritic growth, $\varepsilon=0$. (b) A transition between seaweed and symmetric dendritic growth morphologies occurs for $\varepsilon_c \approx 0.002$. (b) Fully developed symmetric dendritic growth, $\varepsilon=0.012$. Undercooling $\delta T$ equals 0.013. Color map indicates Cu volume fraction so that bright orange areas correspond to crystallized regions rich in Ni.

symmetric dendrite shown in Fig. 1(c) [8]. The position of the advancing dendrite tip spontaneously oscillates in the course of growth for this morphology where the period of oscillation depends on the extent of undercooling, composition, and film thickness $h$ [8]. Crystallization patterns similar to Fig. 1(c) are obtained for $h>80$ nm, but the spontaneous growth pulsations *cease to occur* in thinner films [8], resulting in the morphology change illustrated in the inset to Fig. 1(c). The inset figure has the same composition (30/70) as the thicker film, but $h\approx 50$ nm rather than 200 nm. Notably, the thin-film (50 nm) crystallization pattern has a much more disordered appearance than the thicker film growth patterns [8], showing the impact of the growth pulsations.

The crystallization of the blend film at still lower PEO concentrations is expected to lead to irregular dendritic growth [16] and we indeed observe a reentrant transition from symmetric to branched (*fractal dendritic*) growth upon lowering the PEO concentration to the range 25/75–15/85. The crystallization morphology in Fig. 1(d) is for a 20/80 relative composition film. This growth pattern resembles diffusion-limited aggregation (DLA) [17], but patterns of this form can also be obtained by successive nucleation events at the boundary of a growing crystal [18]. Similar crystallization patterns are commonly found in metallic films [19].

Studies were also made of the blend film crystallization morphologies as a function of $T$. For low undercooling ($\delta T = 0.038$), for example, we observe the growth of near-equilibrium square crystals (image not shown) over long time scales for 30/70 composition blend films and the symmetric dendritic crystallization pattern [Fig. 1(c)] emerges with increasing $\delta T$. Unfortunately, the crossover between these morphologies seems to be a matter of kinetics rather than the magnitude of $\delta T$ (the time over which the Mullins-Sekerka instability disrupts the equilibrium crystallization pattern growth becomes shorter with increased $\delta T$), so that it is difficult to determine the morphology as a function of $T$.

We can obtain some insight into the progression of polymer crystallization morphologies by comparing to simulations of dendritic crystallization in two-dimensional fluid mixtures. Recently, there have been advances in modeling nonequilibrium crystallization using the *phase field* method [20] and Fig. 2 illustrates some phase field simulations dendritic growth where $\varepsilon$ is varied to obtain representative crystallization morphologies. The model parameters in our calculations, apart from the value of $\varepsilon$, are taken to be exactly those chosen in Ref. [20] for a Ni-Cu alloy with a average Cu volume fraction $\phi_{\mathrm{Cu}}=0.408$. (Each run took several hours on a consumer grade personal computer running a Linux operating system [5].) This mixture is miscible and the equilibrium crystals have a square form [13], as the case of PEO. The simulation in Fig. 2 corresponds to a $T$ where the pure Ni crystallizes and the pure Cu does not (PEO crystallizes upon cooling, but PMMA remains amorphous). Further information about the properties of Ni and Cu and simulation parameters are described in Ref. [20]. The color map in Fig. 2 indicates the Cu volume fraction. Orange corresponds to a relatively low concentration of Cu ($\phi_{\mathrm{Cu}}=0.385$) and thus to a relatively high concentration of Ni. Figure 2(a) considers

the extreme case of $\varepsilon = 0$ (isotropic surface tension) where seaweed dendritic growth occurs. In this morphology, the dendrite arms regularly split along the direction of tip propagation and grow in a disorderly fashion without the guidance of anisotropy in the surface tension. This growth pattern clearly resembles the polymer crystallization pattern in Fig. 1(b). Note that both the simulated and blend film seaweed patterns share an early stage of uniform growth, before settling into the tip-splitting mode. This instability [2,21] is less pronounced for larger $\varepsilon$ and a transition from the seaweed to symmetric dendritic growth occurs near $\varepsilon = \varepsilon_c \approx 0.002$. [Both the simulated and polymer dendrites exhibit interesting coexistence between the tip splitting and stable parabolic tip growth for $\varepsilon \approx \varepsilon_c$ and the transitional polymer composition (45/55) in the blend films, respectively, but space limitations do not allow a discussion of this phenomenon here.] Fully developed symmetric dendritic growth is obtained for $\varepsilon \gg \varepsilon_c$ and Fig. 2(b) illustrates this symmetric dendrite growth pattern for $\varepsilon = 0.012$. Notice that the sidebranches grow perpendicularly to the slender paraboloid dendrite arms for large $\varepsilon$. In previous work [20], $\varepsilon$ was fixed somewhat arbitrarily to a large value ($\varepsilon = 0.04$) to mimic dendritic structures seen in the metallurgical mixtures. Of course, these dendrites have a more symmetric appearance than Fig. 2(b). Our main point in showing Fig. 2 is to illustrate the impact of increasing $\varepsilon$ on the structure of dendritic growth patterns. Notably, $\varepsilon$ has never been determined for a polymeric fluid so that more quantitative comparisons of our measurements to the phase field model are not yet possible.

It is apparent that some aspects of the polymer crystallization patterns can be understood from the phase field simulations, while others cannot. The simulations capture the effect of the transition between the seaweed and symmetric dendrite morphologies. This transition has its origin in the variation of $\varepsilon$ in the simulations and varying polymer composition in the polymer blend. The interfacial tension of the blend film is low because of its proximity to a phase boundary for phase separation [7]. An explanation of the ubiquitous ''dense branching'' or spherulite morphology at high PEO concentration remains a puzzle, but our understanding of this morphology in the case of electrodeposition [10] points to elastic effects of the polymer film as being important. At low PEO concentrations, we observe fractal growth patterns reflecting the heterogeneous transport process by which PEO segregates to the growing dendrite. This regime is difficult to simulate using the phase field method because of the enormous separation of time scales associated with the interface attachment kinetics and mass diffusion and because of the highly diffuse nature of the interfaces. Since the slow rate of diffusion can be expected to predominate in this regime, it is sensible to revert to a simpler computational method such as DLA to describe the crystallization process. However, the adoption of such a model causes us to lose contact with the thermodynamic theory that forms the basis of the phase field methodology.

Future work should focus on the growth dynamics of spherulites (e.g., investigate whether the stress field around the growing dendrite exhibits oscillations related to the growth velocity and branching frequency of the needlelike crystallites) and corresponding phase field simulations incorporating elasticity and viscoelastic effects (e.g., shear thinning) are needed to interpret the spherulite growth measurements.

We thank Bernard Lotz (ICS, Strasbourg, France) for helpful comments. We also thank Ronald Heddon and Charles Guttman of the Polymers Division at NIST for characterizing the polydipersity of our PEO and PMMA samples.

[1] Ben Jacob *et al.*, Physica A **187**, 378 (1992).
[2] T. Ihle and H. Müller-Krumbhaar, Phys. Rev. E **49**, 2972 (1994). $\varepsilon$ is the amplitude of the angular $\theta$ dependent contribution to the surface tension, $\gamma = \gamma_0[1 + \varepsilon \cos(k\theta)]$.
[3] M. E. Glicksman *et al.*, Phys. Rev. Lett. **73**, 573 (1994); A. Dougherty *et al.*, *ibid.* **58**, 1652 (1980).
[4] B. Ermi *et al.*, J. Polym. Sci [B] **36**, 191 (1998); L. Sung *et al.*, Phys. Rev. Lett. **76**, 4368 (1996).
[5] Certain commercial materials and equipment identified in this paper do not imply recommendation by NIST.
[6] Molecular weight $M_w$ is more properly termed relative molecular mass.
[7] V. Ferreiro *et al.*, Macromol. Symp. **167**, 73 (2001). Residual chloroform in the cast film is expected to have a strong influence on the film miscibility and polymer mobility.
[8] V. Ferreiro *et al.*, Phys Rev. E (to be published).
[9] B. Wunderlich, *Macromolecular Physics* (Academic, New York, 1976), Vols. 1 and 2.
[10] V. Fleury *et al.*, Nature (London) **367**, 435 (1994).
[11] T. Ihle *et al.*, Phys. Rev. Lett. **70**, 3083 (1993).
[12] B. Utter, *et al.*, Phys. Rev. Lett. **86**, 4604 (2001).
[13] J. Chen *et al.*, J. Polym. Sci. B **33**, 1851 (1995); A. J. Kovacs *et al.*, J. Macromol. Sci., Phys. **B3**, 385 (1969). PEO has monoclinic lattice cell and a 7/2 helix chain conformation. Solution and melt grown crystals grow as square-shaped crystals under near-equilibrium conditions.
[14] P. H. Till, J. Polym. Sci. **24**, 301 (1957); H. D. Keith and F. J. Padden, *ibid.* **39**, 123 (1959). Symmetric dendritic growth has been observed for many years for the crystallization of polymers from solution on surfaces.
[15] L. M. Williams *et al.*, Phys. Rev. E **48**, 489 (1993).
[16] H. Honjo *et al.*, Phys. Rev. Lett. **55**, 841 (1985).
[17] P. Meakin, in *Phase Transitions and Critical Phenomena*, edited by C. Domb and J. L. Lebowitz (Academic Press, New York, 1988), Vol. 12, p. 335.
[18] W. Zi-gin and L. Boquan, Phys. Rev. E **51**, R16 (1995).
[19] H. Jian-guo and W. Zi-gin, Phys. Rev. B **42**, 3271 (1990).
[20] J. A. Warren *et al.*, Acta Metall. Mater. **43**, 689 (1995).
[21] E. Brener *et al.*, Phys. Rev. Lett. **15**, 1978 (1991).